Biomechanical analysis of unilateral biportal endoscopic lumbar interbody fusion: different heights of cage and osteoporosis

Jia-Rui Li
Third Hospital of Shanxi Medical University, Shanxi Academy of Medical Sciences, Tongji Shanxi Hospital

Yang Yan
Taiyuan University of Technology

Xiao-Gang WU
Taiyuan University of Technology

Li-Ming He
Third Hospital of Shanxi Medical University, Shanxi Academy of Medical Sciences, Tongji Shanxi Hospital

Hao-Yu Feng (fenghaoyuspine@126.com)
Third Hospital of Shanxi Medical University, Shanxi Academy of Medical Sciences, Tongji Shanxi Hospital

Research Article

Keywords: lumbar, Unilateral Biportal Endoscopic, lumbar interbody fusion, osteoporosis, finite element analysis

Posted Date: September 6th, 2022

DOI: https://doi.org/10.21203/rs.3.rs-2021910/v1

Abstract

Background

By establishing a finite element model of unilateral biportal endoscopic lumbar interbody fusion (UBE-LIF), the biomechanical characteristics of UBE-LIF technology were analysed and evaluated. The risk of cage subsidence was also evaluated.

Methods

The finite element model of the L4-L5 vertebral body was constructed based on CT data from healthy adult male volunteers. According to the UBE-LIF surgical method, the fusio model with different cage heights of 8 mm, 10 mm and 12 mm was successively constructed. The flexion, extension, right lateral bend, left lateral bend, right axial rotation, and left axial rotation motions were simulated in 6 models with different bone conditions on the upper surface of L4 with 500 N followed load and 10 Nm torsional torque. The range of motion(ROM), Pedicle screw-rod system stress and endplate stress of each model under different working conditions were observed and analysed.

Results

The ROM of the 12mm model was the lowest, simultaneously, the maximum stress of the pedicle screw-rod system of the 12mm model was the lowest. However, the 12mm model has the largest endplate stress. The maximum stress of the L4 inferior endplate was greater than that of the L5 superior endplate in the UBE-LIF surgical models (24.9%). Compared with the normal model, the ROM of the osteoporosis model increased by 4.7%, the maximum stress of the pedicle screw-rod system increased by 14%, and the maximum stress of the endplate increased by 7.5%.

Conclusions

The results show that the appropriate height of the cage should be selected during the operation to ensure the stability of the segment and avoid the risk of the subsidence caused by the high cage. This is especially important for patients with osteoporosis.

1. Introduction

Degenerative diseases of the lumbar spine include lumbar disc herniation and lumbar spinal stenosis, which cause clinical symptoms such as low back pain, radiating pain of the lower limbs and intermittent claudication and affect patients' quality of life[1]. They are common clinical diseases[2].

Open lumbar posterior fusion is considered a routine surgical approach for the treatment of degenerative diseases of the lumbar spine. It restores the stability of the lumbar spine and improves the height of the lumbar intervertebral space while completely decompressing the neural structures and has been proven to be safe and effective[3]. Open surgery, however, requires extensive dissection and injury of the paraspinal muscles, as well as destruction of the posterior structures of the lumbar spine, resulting in iatrogenic lower back pain due to trauma and bleeding[4, 5]. UBE-LIF technology combines the advantages of endoscopy and open fusion surgery to propose a minimally invasive surgical approach to lumbar interbody fusion[6].

Although minimally invasive surgery has the advantages of reducing trauma and speeding up postoperative recovery[7], cage subsidence cannot be completely avoided. cage subsidence will lead to narrowing of the intervertebral space, affect the stability of the spine, and even lead to fusion failure, adjacent segment degeneration and other serious consequences[8]. It has been reported that the cage subsidence rate in posterior fusion surgery is approximately 34.1% to 59.3%[9, 10]. The risk factors that cause the subsidence are the size, shape and material of the cage[11, 12], the position of the cage[13], body mass index (BMI)[14], disc height [15], and osteoporosis (as an independent risk factor, which not only easily leads to degenerative changes in the lumbar spine but also increases the risk of subsidence by more than 1.3 times)[16, 17]. In current clinical studies, the follow-up time for UBE-LIF varies, and there are few reports on the incidence of cage subsidence.

The finite element analysis method can simulate the surgical model and evaluate the risk of cage subsidence by analysing the data. Fan et al.'s compared two finite element models, transforaminal lumbar interbody fusion (TLIF) and posterior lumbar interbody fusion (PLIF), it was found that the endplate stress of TLIF was 29.2% higher than that of PLIF (its subsidence risk is greater)[18]. In the finite element model of TLIF surgery, both the 10 mm cage and 8 mm cage were placed. Compared with the stress of the endplate, the 10 mm cage increased by 16%, which proved that the risk of subsidence increased with higher cage placement[19]. Park et al.'s established a TLIF surgical model of osteoporosis and found that the risk of subsidence was significantly increased[20]. The results of these studies are similar to those of clinical studies[21], indicating that the finite element analysis method is of certain reference value to study the risk of subsidence.

Therefore, the UBE-LIF finite element model was established in this study, and two factors, including different cage heights and osteoporosis, were set to evaluate the risk of cage subsidence. The purpose of this study is to provide a reference for selecting the height of the cage during UBE-LIF operation.

2. Materials And Methods

2.1 Normal finite element model construction of L4-5

2.1.1 Subjects

A normal adult male was selected as a volunteer. There was no history of lumbar pain, trauma or surgery, and lumbar lesions were excluded through imaging.

2.1.2 Collection device

Siemens Third Generation SOMATOM Force CT (Bethune Hospital, Shanxi)

2.1.3 sampling

A healthy young male volunteer was selected to participate in the experiment. CT tomography along the superior edge of the L1 vertebral body to the inferior edge of the S1 vertebral body was selected with a thickness of 0.75 mm.

2.1.4 Method

According to the vertebral body contour in CT data, L4-5 vertebral bodies were extracted. According to the mechanical material properties of various lumbar structures in previous studies, cortical bone, cancellous bone, posterior structure, bone endplate, cartilage endplate, intervertebral disc, nucleus pulpous, facet joint and 7 major ligaments were constructed successively. These included the anterior longitudinal ligament ALL , posterior longitudinal ligament PLL , ligamentum flava LF , capsular ligament CL , intertransverse ligament ITL , interspinous ligament ISL and supraspinous ligament SSL [22]. The cortical bone was set as a shell unit of 1.0 mm thickness. The superior and inferior surfaces of the vertebral body were constructed with cartilage endplates of 0.5 mm thickness and bone endplates of the same thickness. The 3D tetrahedral mesh technique was applied to each structure, which was treated with common nodes compared with neighbouring structures **(Figure 1A)**.

The annulus fibrosus and nucleus pulpous were set as Mooney-Rivlin hyperelastic materials; that is, collagen fibres as one-dimensional spring elements only work under tension **(Figure 1B)**. Ligaments are simulated using TRUSS units and can only withstand tension, not stress. The rest were set as isotropic homogeneous elastic materials[23].

Facet joint surfaces were set to face-to-face contact, and their property was set to tangential action without friction, with normal action to hard friction as a "penalty" function. A binding contact was established at the attachment site of the ligament and cortical bone.

2.2 Setting of osteoporosis model

The osteoporotic model simulated the material properties of osteoporosis by reducing the Young's modulus of bone. The material properties of osteoporosis are defined as a 66% reduction in Young's

modulus of cancellous bone and a 33% reduction in Young's modulus of cortical bone, bony endplate and posterior structure, while the soft tissue structure remains unchanged **(Figure 2)**[24].

2.3 Establishment of a finite element model of L4-5 UBE-LIF surgery

On the basis of the normal model, the left inferior articular process of L4, left superior articular process of L5, left facet articular capsule, left capsule ligament, 30% of the posterior longitudinal ligament, 50% of the ligamentum flavum, all of the nucleus pulpous and 10% of the annular fibre were removed. The UBE-LIF procedure was simulated[25].

The cage model was set to 26 mm and 10 mm in length and width, respectively. Bone mud from autogenous cancellous bone was filled inside the cage (13 mm*5 mm).

After measuring and adjusting the L4-5 intervertebral space height, cages with heights of 8mm, 10mm and 12mm was placed between the L4-5 endplates at an Angle of 30° through an intervertebral foramen approach **(Figure 3A)**[26].

The interface between the adjacent endplate and the cage was set as a face-to-face contact with a friction coefficient of 0.5. The posterior percutaneous pedicle screw placement technique was simulated., four pedicle screws (45 mm in length, 6.5 mm in diameter) were inserted posterior to the L4 and L5 vertebral body, and titanium rods (55 mm in length, 5.5 mm in diameter) were connected to the ends of the ipsilateral screws for fixation **(Figure 3B)**. The cage, pedicle screw and rod were all made of titanium alloy (Ti6Al4 V), and the screw had binding with the vertebral body. Its material parameters were obtained from previous literature reports[27, 28], as shown in **Tables 1 and 2.**

Table 1. Lumbar spine results and internal fixation material attribute parameters

Structures	Young's modulus (MPa)	Poisson's ratio	Element type
Cortical bone normal	12000	0.30	C3D4
Cortical bone osteoporotic	8040	0.30	C3D4
Cancellous bone normal	100	0.20	C3D4
Cancellous bone osteoporotic	34	0.20	C3D4
Posterior element normal	3500	0.30	C3D4
Posterior element osteoporotic	2345	0.30	C3D4
Bony endplate normal	2000	0.20	C3D4
Bony endplate osteoporotic	1340	0.20	C3D4
Cartilage endplate	24	0.30	C3D4R
Annulus fibrosus	Mooney-Rivlin C1=0.18 C2=0.045	-	C3D4
Nucleus pulpous	Mooney-Rivlin C1=0.12 C2=0.03	-	C3D4RH
Facet joint	10000	0.30	C3D4RH
Cage Ti6Al4V	110000	0.30	C3D4RR
Bone graft normal	100	0.20	C3D4R
Bone graft osteoporotic	34	0.20	C3D4R
Pedicle screws-rod Ti6Al4V	110000	0.30	C3D4

Table 2. Attribute parameters of 7 lumbar ligament materials

Ligaments	Young's modulus (MPa)	Poisson's ratio	Element type	Cross-sectional Area (mm^2)
ALL	7.8	0.30	T3D2	76
PLL	1	0.30	T3D2	15
LF	1.5	0.30	T3D2	40
ITL	10	0.30	T3D2	3
CL	7.5	0.30	T3D2	30
ISL	1	0.30	T3D2	30
SSL	3	0.30	T3D2	23

By assigning material attributes to each model and structure, we generated:

1. L4-5 normal 3D finite element Model (N0),
2. Finite element model of L4-5 osteoporosis (S0),
3. Normal UBE-LIF model with an 8 mm cage in L4-5 (N1)
4. UBE-LIF model of osteoporosis with an 8 mm cage in L4-5 (S1),
5. Normal UBE-LIF model with a 10 mm cage in L4-5 (N2),
6. UBE-LIF model of osteoporosis with a 10 mm cage in L4-5 (S2),
7. Normal UBE-LIF Model with a 12 mm cage in L4-5(N3),
8. UBE-LIF model of osteoporosis with a 12 mm cage in L4-5 (S3).

2.4 Setting of boundary and load conditions

Each model involved the following: torque and load on the L4 vertebral body on the upper surface of the coupling nodes, completely fixed constraint at the bottom of the L5 vertebral bodies of six degrees of freedom, the model of L4 vertebral body surface coupling point on follower-load of 500 N, simulation of the half body weight and waist muscle tissue of the compression load produced by the synergy and application of 10 Nm torque coupling points[29], with six lumbar postures, such as flexion, extension, left lateral bending, right lateral bending ,left axial rotation, right axial rotation **(Figure 4)**.

2.5 Main outcome measures

The relative ROMs of the L4-5 segments, the maximum stress of the Pedicle screw-rod system and the maximum stress distribution between the L4-5 endplates of the cage were observed and recorded under

different motion states.

3. Results

3.1 Validity verification and biomechanical evaluation of the model

The ROMs of the L4-5 model under 6 different working conditions was measured by applying the above boundary and loading conditions to the normal lumbar finite element Model (N0). The results were compared with those of laboratory cadavers[30]. The results show that the trend is consistent **(Figure 5)**, and the biomechanical measurement is within one standard deviation, indicating that the N0 finite element model can be used in relevant studies. This indicated that model verification had succeeded.

3.2 Biomechanical evaluation of cage implantation at different heights

3.2.1 ROM

The biomechanical characteristics of six UBE-LIF finite element models were compared, and the motion of each model under general physiological motion was simulated, namely, flexion, extension, bending and rotation. The ROMs of L4-5 is shown in **Figure 6**.

The ROMs of the N0 model were 6.2°, 3.2°, 5.1°, 5°, 5° and 5.1° under flexion, extension, left lateral bending, right lateral bending, left axial rotation, right axial rotation, respectively. The ROMs of the S0 model were 6.6°, 3.5°, 5.4°, 5.2°, 5.3° and 5.3° under flexion, extension, left lateral bending, right lateral bending, left axial rotation, right axial rotation. respectively, which were much higher than the ROMs after UBE-LIF.

The maximum values of ROMs of the six UBE-LIF surgical models all appeared in the flexion movement, and the minimum values appeared in the extension movement. The ROMs of the six UBE-LIF models in the right lateral bending were all larger than those in the left lateral bending, and the ROMs in the right axial rotation were all larger than those in the left axial rotation.

Under normal conditions of bone mass, ROMs at the L4-5 was decreased in all three UBE-LIF surgical models compared with the N0 model, and ROM in the N3 model was the lowest. ROM in the N2 model increased by 7% compared with the N3 model, and ROM in the N1 model increased by 10% compared with the N2 model. Osteoporosis was similar to the normal bone mass model. The S3 model had the lowest ROM, ROM in the S2 model increased by 12% compared with the S3 model, and ROM in the N1 model increased by 7% compared with the N2 model. When the height of the cage is the same, the ROMs

of the osteoporosis model was slightly higher than that of the normal bone mass model (approximately 4.7%).

3.2.2 Maximum stress of the Pedicle screw-rod system

The biomechanical characteristics of the six UBE-LIF models were compared, and the movement of each model under general physiological movement, namely, flexion, extension, bending and rotation, was simulated. The stress distribution of the screw-rod system is shown in **Figure 7 and 8.**

Under normal conditions, the maximum stress of N3(167~284Mpa was the smallest, N1 (253~337Mpa maximum stress being 14% larger than N2(214~274Mpa maximum stress, N2 maximum stress being 9% larger than N3 maximum stress, and N1 maximum stress being 24% larger than N3 maximum stress.Under Osteoporosis conditions, the maximum stress of S3(168~288Mpa model was the smallest, S1(267~444Mpa maximum stress being 18% larger than S2(228~325Mpa maximum stress, S2 maximum stress being 22% larger than S3 maximum stress, and S1 maximum stress being 50% larger than S3 maximum stress.

In terms of the maximum stress of the Pedicle screw-rod system, the stress of the six UBE-LIF models reached the maximum in the simulation of lateral bending and the minimum in the simulation of flexion and extension. and the maximum stress was greater in left lateral bending than in right lateral bending, left axial rotation than in right axial rotation, and extension than in flexion.

The maximum stress of the osteoporotic model was higher than that of the normal bone mass model when the same height of the cage (approximately 14%).

3.2.3 Maximum stress of the endplate

The biomechanical characteristics of the six UBE-LIF models were compared, and the motion of each model under general physiological motion was simulated, namely, flexion, extension, bending and rotation. the maximum stress distribution of the inferior endplate of L4 and the superior endplate of L5 were shown in Figure 9, 10 and 11.

In the normal bone mass model, In the inferior endplate of L4, the maximum stress of N1 endplate was the lowest(16~33.6Mpa , N2 maximum stress 20.7~42.4Mpa increased by 45% compared with N1 maximum stress, N3 maximum stress 30.2~70.6Mpa increased by 63% compared with N2 maximum stress, and N3 maximum stress increased by 136% compared with N1 maximum stress. The superior endplate of L5, the maximum stress of the N1 endplate was also the lowest 12.4~21.5Mpa , N2 maximum stress 17~41Mpa increased by 39% compared with N1 maximum stress. N3 maximum stress 23.2~65.9Mpa increased by 58% compared with N2 maximum stress, and N3 maximum stress increased by 121% compared with N1 maximum stress.

In the osteoporosis model, In the inferior endplate of L4, the maximum stress of S1 endplate was the lowest 15.8~34.6Mpa , S2 maximum stress 22~45.4Mpa increased by 47% compared with S1 maximum stress, S3 maximum stress 33.2~72.8Mpa increased by 61% compared with S2 maximum stress, and S3 maximum stress 32.2~71.8Mpa increased by 139% compared with S1 maximum stress. The superior endplate of L5, the maximum stress of the S1 endplate was also the lowest 14.5~24.1Mpa , S2 maximum stress 19.8~43.2Mpa increased by 45% compared with S1 maximum stress. S3 maximum stress 31.2~69.2Mpa increased by 63% compared with S2 maximum stress, and S3 maximum stress increased by 138% compared with S1 maximum stress.

When the height of the cage is the same, the maximum stress between the cage and the adjacent endplate in the osteoporosis model was slightly more than that in the normal bone mass model (approximately 7.5%). The maximum stress of the inferior endplate of L4 was greater than that of the superior endplate of L5 in the six UBE-LIF surgical models under six motion modes (approximately 24.1%). the maximum stress of the inferior endplate of L4 was the maximum during flexion motion, and the stress of the endplate was the minimum during extension motion.

4. Discussion

As a new minimally invasive fusion technique, UBE-LIF can not only improve the surgical field through endoscopy but also provide the same flexibility and efficacy of open surgery[31]. To minimize posterior muscle dissection and ligament damage, direct decompression of the spinal canal and bilateral nerve roots was performed through excision of the ligamentum flava, lamina and facet, while an interbody fusion cage was inserted to restore the lumbar sequence and provide immediate stability[32]. At present, clinical studies on the operation and postoperative efficacy of UBE-LIF technology are extensive, but there are few reports on cage subsidence[33, 34]. Therefore, we used the finite element analysis method to conduct biomechanical analysis on the risk of postoperative cage subsidence of UBE-LIF with different bones and different heights of cage. The results showed that patients with osteoporosis had a higher risk of subsidence after UBE-LIF surgery. An increase in the height of the cage will improve the stability of the segment, but the risk of the subsidence will also increase.

The ROMs of the UBE-LIF model was significantly lower than that of the normal lumbar model under all six motion states, suggesting that UBE-LIF enhanced the stability of the segment. Part of the L4-5 left structure was removed in the UBE-LIF model, and the ROMs of the model after surgery was larger in the right bend and right rotation than in the left bend and left rotation. Patients with UBE-LIF should pay attention to their movements to protect their spines

The ROM of the 12 mm cage model was minimal, and the maximum stress of the pedicle screw-rod system was minimal. The reasons are as follows: with the expansion of the intervertebral space height, the nonlinear pull protection of the seven ligaments is enhanced, while the restoration of lumbar lordotic angle improves the stability of the entire spine[35].

In this study, ROMs of segments was significantly increased in patients with osteoporosis[36]. The maximum stress of the pedicle screw-rod system increased significantly. Previous experiments have proven that the cancellous bone mineral density in patients with osteoporosis is very significant[37]. However, pedicle screw fixation mainly depends on the bone density of cancellous bone, according to the experimental conclusion of Chen et al.[38], when the maximum stress of the pedicle screw exceeds the yield stress of the cancellous bone by 343.5MPa, the cancellous bone will be destructed and the pedicle screw will be loosened. Combined with the results of this study, the 8mm osteoporosis model has the maximum stress exceeding the yield stress during lateral bending, so screw loosening may be greater in osteoporosis patients. Therefore, patients with osteoporosis need strict anti-osteoporosis treatment after surgery[39].

In the UBE-LIF model, the maximum stress of the inferior endplate of L4 was greater than that of the superior endplate of L5, and the stress increased with increasing height of the cage. Previous finite element studies showed that subsidence occurred because the von-Mises stress value of the adjacent endplate reached the failure stress value of the vertebral body itself[40, 41]. Wu et al.'s experimental results show that the yield stress of L4 inferior endplate is 27.49 ± 11.60 MPa, and The L5 superior endplate is 38.26 ± 19.28 MPa[42].Combined with the results of this study, In the L4 inferior endplate, the 8mm model does not exceed the yield stress, the 10mm model has the maximum stress exceeding the yield stress during flexion, while the 12mm model has only the extension not exceeding the yield stress. In the L5 superior endplate, the 8mm model and the 10mm model do not exceed the yield stress, and the 12mm model has the maximum stress exceeding the yield stress during flexion. Therefore, the higher the height of the cage, the higher the risk of subsidence in the inferior endplate of L4. Fan et al.'s finite element analysis of anterior lumbar interbody fusion (ALIF), PLIF and TLIF also proved this[43]. In this study, the maximum stress of the endplate in the osteoporosis model was approximately 7.5% more than that in the normal model. Analysis showed that this was because the bone structural strength of osteoporosis patients decreased significantly, Osteoporotic cortical bone and cancellous bone density decreases affect bone stiffness and strain values[44]. and the bone stiffness decreased by 14% on average[45].Decreased bone stiffness increases the risk of cage subsidence[46]. In this study, it was found that the stress peak of the endplate all occurred in the state of flexion, suggesting that postoperative patients should wear waist circumference protector to avoid excessive lumbar flexion.

By comparing the biomechanics of the UBE-LIF model, we found that the ROM of the surgical segment was reduced by 7% in the 10 mm cage model compared with the 8 mm cage model, and the maximum stress of the pedicle screw-rod system was reduced by 14%, but the maximum stress of the L4 inferior endplate and the L5 superior endplate was increased by 45% and 39%, respectively. In the 12 mm cage model, compared with the 10 mm cage model, the ROM of the surgical segment was reduced by 10%, and the maximum stress of the pedicle screw-rod system was reduced by 9%, but the maximum stress of the L4 inferior endplate and the L5 superior endplate increased by 63% and 58%, respectively. The use of a larger cage significantly increased the maximum stress of the endplate and increased the risk of cage subsidence, although it reduced the mobility of the segments and the maximum stress of the pedicle screw-rod system, improving the stability of the surgical segments and the pedicle screws. Previous

studies have shown that the greater the lumbar intervertebral space after Extreme lateral interbody fusions (XLIF), the greater the probability of postoperative subsidence[47]. After TLIF, the height of the cage was greater than the height of the lumbar space by 1.3 mm, and the sensitivity of subsidence was 93.3%[48]. This indicates that the choice of the high height of the cage is bound to increase the risk of cage subsidence, while the choice of the small height of the cage cannot restore the curvature and stability of the lumbar spine. Therefore, the selection of the appropriate height of the cage is of great significance to reduce the postoperative cage subsidence. Compared with the traditional static cage, the new expandable interbody fusion cage can be adjusted in real time after intervertebral space placement according to the feedback resistance and intraoperative imaging detection in the process of distraction to avoid excessive distraction height of the cage and effectively restore the lumbar space height and lordotic angle[49]. Cadaver experiments have shown that the expandable cage can significantly improve sagittal balance and thus enhance segmental stability[50]. The expandable cage was used in the UBE-LIF operation, and good results were obtained after the operation[51]. Combined with the results of this study and other related studies, it is proven that the expandable cage may improve the stress condition of the endplate and reduce the risk of subsidence.

In this study, finite element analysis of the three-dimensional lumbar spine model was used to restore the biomechanics of the lumbar spine after UBE-LIF surgery to a certain extent, and simulation analysis was conducted on different lumbar intervertebral space heights. However, there are still some limitations in the research results. First, the lumbar model was established based on healthy subjects without spinal disease, without considering changes in vertebral morphology and structure caused by lesions. Second, we only simulated the reconstruction of the L4-5 vertebral body and some adjacent structures and failed to construct the soft tissue structures, such as paraspinal muscles, in detail. In addition, the elastic modulus and Poisson's ratio obtained in previous literature cannot replace the bone mineral density of the real vertebral body, and there is still a certain gap between them, so they cannot simulate the real biomechanical state of the human body. The results obtained by using the finite element technique can reflect the basic state of the spine and provide a direction for further research.

5. Conclusion

We found that the placement of a high-height cage in UBE-LIF surgery provided better segmental stability and reduced stress in the pedicle screw-rod system. However, higher cages significantly increase the risk of cage subsidence. Patients with osteoporosis have worse postoperative segmental stability, greater stress on the pedicle screw-rod system, and a higher risk of cage subsidence than patients with normal bones. Therefore, the higher the cage is, the better, but it needs to be properly opened to ensure segmental stability while avoiding the increased risk of subsidence caused by an excessively high cage, which is more important for patients with osteoporosis.

Abbreviations

UBE-LIF: unilateral biportal endoscopic lumbar interbody fusion

ROM: range of motion;

BMI: body mass index;

TLIF: transforaminal lumbar interbody fusion;

ALL: anterior longitudinal ligament;

PLL: posterior longitudinal ligament;

LF: ligamentum flava;

CL: capsular ligament;

ITL: intertransverse ligament;

ISL: interspinous ligament;

SSL: supraspinous ligament;

PLIF: posterior lumbar interbody fusion;

ALIF: anterior lumbar interbody fusion;

XLIF: Extreme lateral interbody fusions.

Declarations

Acknowledgements

Not applicable.

Authors' contributions

JRL and YY designed the computer model and performed the finite element analysis and interpretation. HYF and LMH contributed to the conception, design, and data analysis. HYF, LMH and XGW contributed to revise the manuscript. All authors read and approved the final manuscript.

Funding

This work was supported by the Health Commission of Shanxi Province (grant number 2020TD13)

Ethics approval and consent to participate

The study was conducted according to the guidelines of the Declaration of Helsinki and was approved by the Institutional Review Board (or Ethics Committee) of Shanxi Bethune Hospital. Informed consent was obtained from all subjects involved in the study.

Consent for publication

Not applicable.

Availability of data and materials

The datasets used and/or analysed during the current study are available from the corresponding author on reasonable request.

Disclosure statement

No potential conflict of interest was reported by the authors.

References

1. Azimi P, Mohammadi HR, Benzel EC, Shahzadi S, Azhari S. Lumbar Spinal Canal Stenosis Classification Criteria: A New Tool. Asian spine journal. 2015;9(3):399-406.
2. Yasuhara T, Sasada S, Date I. [Lumbar Degenerative Disease:Key for Diagnosis]. No shinkei geka Neurological surgery. 2021;49(6):1233-45.
3. Fleege C, Rickert M, Rauschmann M. [The PLIF and TLIF techniques. Indication, technique, advantages, and disadvantages]. Der Orthopade. 2015;44(2):114-23.
4. Mobbs RJ, Li J, Sivabalan P, Raley D, Rao PJ. Outcomes after decompressive laminectomy for lumbar spinal stenosis: comparison between minimally invasive unilateral laminectomy for bilateral decompression and open laminectomy: clinical article. Journal of neurosurgery Spine. 2014;21(2):179-86.
5. Oppenheimer JH, DeCastro I, McDonnell DE. Minimally invasive spine technology and minimally invasive spine surgery: a historical review. Neurosurgical focus. 2009;27(3):E9.
6. Heo DH, Son SK, Eum JH, Park CK. Fully endoscopic lumbar interbody fusion using a percutaneous unilateral biportal endoscopic technique: technical note and preliminary clinical results. Neurosurgical focus. 2017;43(2):E8.
7. Yang J, Liu C, Hai Y, Yin P, Zhou L, Zhang Y, et al. Percutaneous Endoscopic Transforaminal Lumbar Interbody Fusion for the Treatment of Lumbar Spinal Stenosis: Preliminary Report of Seven Cases with 12-Month Follow-Up. BioMed research international. 2019;2019:3091459.
8. Du JY, Kiely PD, Al Maaieh M, Aichmair A, Huang RC. Lateral lumbar interbody fusion with unilateral pedicle screw fixation for the treatment of adjacent segment disease: a preliminary report. Journal of spine surgery (Hong Kong). 2017;3(3):330-7.
9. Yao YC, Chou PH, Lin HH, Wang ST, Liu CL, Chang MC. Risk Factors of Cage Subsidence in Patients Received Minimally Invasive Transforaminal Lumbar Interbody Fusion. Spine. 2020;45(19):E1279-e85.

10. Singhatanadgige W, Sukthuayat A, Tanaviriyachai T, Kongtharvonskul J, Tanasansomboon T, Kerr SJ, et al. Risk factors for polyetheretherketone cage subsidence following minimally invasive transforaminal lumbar interbody fusion. Acta neurochirurgica. 2021;163(9):2557-65.
11. Igarashi H, Hoshino M, Omori K, Matsuzaki H, Nemoto Y, Tsuruta T, et al. Factors Influencing Interbody Cage Subsidence Following Anterior Cervical Discectomy and Fusion. Clinical spine surgery. 2019;32(7):297-302.
12. Tan JH, Cheong CK, Hey HWD. Titanium (Ti) cages may be superior to polyetheretherketone (PEEK) cages in lumbar interbody fusion: a systematic review and meta-analysis of clinical and radiological outcomes of spinal interbody fusions using Ti versus PEEK cages. European spine journal : official publication of the European Spine Society, the European Spinal Deformity Society, and the European Section of the Cervical Spine Research Society. 2021;30(5):1285-95.
13. Choi WS, Kim JS, Hur JW, Seong JH. Minimally Invasive Transforaminal Lumbar Interbody Fusion Using Banana-Shaped and Straight Cages: Radiological and Clinical Results from a Prospective Randomized Clinical Trial. Neurosurgery. 2018;82(3):289-98.
14. Jones C, Okano I, Salzmann SN, Reisener MJ, Chiapparelli E, Shue J, et al. Endplate volumetric bone mineral density is a predictor for cage subsidence following lateral lumbar interbody fusion: a risk factor analysis. The spine journal : official journal of the North American Spine Society. 2021;21(10):1729-37.
15. Hiyama A, Sakai D, Katoh H, Nomura S, Sato M, Watanabe M. Comparative Study of Cage Subsidence in Single-Level Lateral Lumbar Interbody Fusion. Journal of clinical medicine. 2022;11(5).
16. Derman PB, Ohnmeiss DD, Lauderback A, Guyer RD. Indirect Decompression for the Treatment of Degenerative Lumbar Stenosis. International journal of spine surgery. 2021;15(6):1066-71.
17. Oh KW, Lee JH, Lee JH, Lee DY, Shim HJ. The Correlation Between Cage Subsidence, Bone Mineral Density, and Clinical Results in Posterior Lumbar Interbody Fusion. Clinical spine surgery. 2017;30(6):E683-e9.
18. Fan W, Guo LX, Zhao D. Posterior Lumbar Interbody Fusion Versus Transforaminal Lumbar Interbody Fusion: Finite Element Analysis of the Vibration Characteristics of Fused Lumbar Spine. World neurosurgery. 2021;150:e81-e8.
19. Rastegar S, Arnoux PJ, Wang X, Aubin C. Biomechanical analysis of segmental lumbar lordosis and risk of cage subsidence with different cage heights and alternative placements in transforaminal lumbar interbody fusion. Computer methods in biomechanics and biomedical engineering. 2020;23(9):456-66.
20. Park MK, Kim KT, Bang WS, Cho DC, Sung JK, Lee YS, et al. Risk factors for cage migration and cage retropulsion following transforaminal lumbar interbody fusion. The spine journal : official journal of the North American Spine Society. 2019;19(3):437-47.
21. Heinz von der Hoeh N, Villa T, Galbusera F, Voelker A, Spiegl UA, Jarvers JS, et al. Analysis of a Unilateral Bridging Cage for Lumbar Interbody Fusion: 2-Year Clinical Results and Fusion Rate with a

Focus on Subsidence. World neurosurgery. 2018;116:e308-e14.

22. Liu X, Ma J, Park P, Huang X, Xie N, Ye X. Biomechanical comparison of multilevel lateral interbody fusion with and without supplementary instrumentation: a three-dimensional finite element study. BMC musculoskeletal disorders. 2017;18(1):63.
23. Yu Y, Zhou Q, Xie YZ, Wang XL, Fan XH, Gu DW, et al. Effect of Percutaneous Endoscopic Lumbar Foraminoplasty of Different Facet Joint Portions on Lumbar Biomechanics: A Finite Element Analysis. Orthopaedic surgery. 2020;12(4):1277-84.
24. Li J, Xu W, Zhang X, Xi Z, Xie L. Biomechanical role of osteoporosis affects the incidence of adjacent segment disease after percutaneous transforaminal endoscopic discectomy. Journal of orthopaedic surgery and research. 2019;14(1):131.
25. Heo DH, Hong YH, Lee DC, Chung HJ, Park CK. Technique of Biportal Endoscopic Transforaminal Lumbar Interbody Fusion. Neurospine. 2020;17(Suppl 1):S129-s37.
26. Kim JE, Choi DJ. Biportal Endoscopic Transforaminal Lumbar Interbody Fusion with Arthroscopy. Clinics in orthopedic surgery. 2018;10(2):248-52.
27. He L, Xiang Q, Yang Y, Tsai TY, Yu Y, Cheng L. The anterior and traverse cage can provide optimal biomechanical performance for both traditional and percutaneous endoscopic transforaminal lumbar interbody fusion. Computers in biology and medicine. 2021;131:104291.
28. Zhu H, Zhong W, Zhang P, Liu X, Huang J, Liu F, et al. Biomechanical evaluation of autologous bone-cage in posterior lumbar interbody fusion: a finite element analysis. BMC musculoskeletal disorders. 2020;21(1):379.
29. Vadapalli S, Sairyo K, Goel VK, Robon M, Biyani A, Khandha A, et al. Biomechanical rationale for using polyetheretherketone (PEEK) spacers for lumbar interbody fusion-A finite element study. Spine. 2006;31(26):E992-8.
30. Shim CS, Park SW, Lee SH, Lim TJ, Chun K, Kim DH. Biomechanical evaluation of an interspinous stabilizing device, Locker. Spine. 2008;33(22):E820-7.
31. Heo DH, Lee N, Park CW, Kim HS, Chung HJ. Endoscopic Unilateral Laminotomy with Bilateral Discectomy Using Biportal Endoscopic Approach: Technical Report and Preliminary Clinical Results. World neurosurgery. 2020;137:31-7.
32. Park MK, Park SA, Son SK, Park WW, Choi SH. Clinical and radiological outcomes of unilateral biportal endoscopic lumbar interbody fusion (ULIF) compared with conventional posterior lumbar interbody fusion (PLIF): 1-year follow-up. Neurosurgical review. 2019;42(3):753-61.
33. Heo DH, Sharma S, Park CK. Endoscopic Treatment of Extraforaminal Entrapment of L5 Nerve Root (Far Out Syndrome) by Unilateral Biportal Endoscopic Approach: Technical Report and Preliminary Clinical Results. Neurospine. 2019;16(1):130-7.
34. Kim SK, Kang SS, Hong YH, Park SW, Lee SC. Clinical comparison of unilateral biportal endoscopic technique versus open microdiscectomy for single-level lumbar discectomy: a multicenter, retrospective analysis. Journal of orthopaedic surgery and research. 2018;13(1):22.

35. Claeson AA, Barocas VH. Computer simulation of lumbar flexion shows shear of the facet capsular ligament. The spine journal : official journal of the North American Spine Society. 2017;17(1):109-19.
36. Sebaaly A, Grobost P, Mallam L, Roussouly P. Description of the sagittal alignment of the degenerative human spine. European spine journal : official publication of the European Spine Society, the European Spinal Deformity Society, and the European Section of the Cervical Spine Research Society. 2018;27(2):489-96.
37. Löffler MT, Sollmann N, Mei K, Valentinitsch A, Noël PB, Kirschke JS, et al. X-ray-based quantitative osteoporosis imaging at the spine. Osteoporosis international : a journal established as result of cooperation between the European Foundation for Osteoporosis and the National Osteoporosis Foundation of the USA. 2020;31(2):233-50.
38. Chen HC, Wu JL, Huang SC, Zhong ZC, Chiu SL, Lai YS, et al. Biomechanical evaluation of a novel pedicle screw-based interspinous spacer: A finite element analysis. Medical engineering & physics. 2017;46:27-32.
39. Bae JS, Lee SH, Kim JS, Jung B, Choi G. Adjacent segment degeneration after lumbar interbody fusion with percutaneous pedicle screw fixation for adult low-grade isthmic spondylolisthesis: minimum 3 years of follow-up. Neurosurgery. 2010;67(6):1600-7; discussion 7-8.
40. Hansen U, Zioupos P, Simpson R, Currey JD, Hynd D. The effect of strain rate on the mechanical properties of human cortical bone. Journal of biomechanical engineering. 2008;130(1):011011.
41. Yeni YN, Hou FJ, Vashishth D, Fyhrie DP. Trabecular shear stress in human vertebral cancellous bone: intra- and inter-individual variations. Journal of biomechanics. 2001;34(10):1341-6.
42. Wu Y, Loaiza J, Banerji R, Blouin O, Morgan E. Structure-function relationships of the human vertebral endplate. JOR spine. 2021;4(3):e1170.
43. Fan W, Guo LX. Biomechanical comparison of the effects of anterior, posterior and transforaminal lumbar interbody fusion on vibration characteristics of the human lumbar spine. Computer methods in biomechanics and biomedical engineering. 2019;22(5):490-8.
44. Westbury LD, Shere C, Edwards MH, Cooper C, Dennison EM, Ward KA. Cluster Analysis of Finite Element Analysis and Bone Microarchitectural Parameters Identifies Phenotypes with High Fracture Risk. Calcified tissue international. 2019;105(3):252-62.
45. Polikeit A, Nolte LP, Ferguson SJ. The effect of cement augmentation on the load transfer in an osteoporotic functional spinal unit: finite-element analysis. Spine. 2003;28(10):991-6.
46. Formby PM, Kang DG, Helgeson MD, Wagner SC. Clinical and Radiographic Outcomes of Transforaminal Lumbar Interbody Fusion in Patients with Osteoporosis. Global spine journal. 2016;6(7):660-4.
47. Kaliya-Perumal AK, Soh TLT, Tan M, Oh JY. Factors Influencing Early Disc Height Loss Following Lateral Lumbar Interbody Fusion. Asian spine journal. 2020;14(5):601-7.
48. Pisano AJ, Fredericks DR, Steelman T, Riccio C, Helgeson MD, Wagner SC. Lumbar disc height and vertebral Hounsfield units: association with interbody cage subsidence. Neurosurgical focus. 2020;49(2):E9.

49. Cappelletto B, Giorgiutti F, Balsano M. Evaluation of the effectiveness of expandable cages for reconstruction of the anterior column of the spine. Journal of orthopaedic surgery (Hong Kong). 2020;28(1):2309499019900472.
50. Pekmezci M, Tang JA, Cheng L, Modak A, McClellan RT, Buckley JM, et al. Comparison of expandable and fixed interbody cages in a human cadaver corpectomy model, part I: endplate force characteristics. Journal of neurosurgery Spine. 2012;17(4):321-6.
51. Yao N, Wang W, Liu Y. Percutaneous endoscopic lumbar discectomy and interbody fusion with B-Twin expandable spinal spacer. Archives of orthopaedic and trauma surgery. 2011;131(6):791-6.

Figures

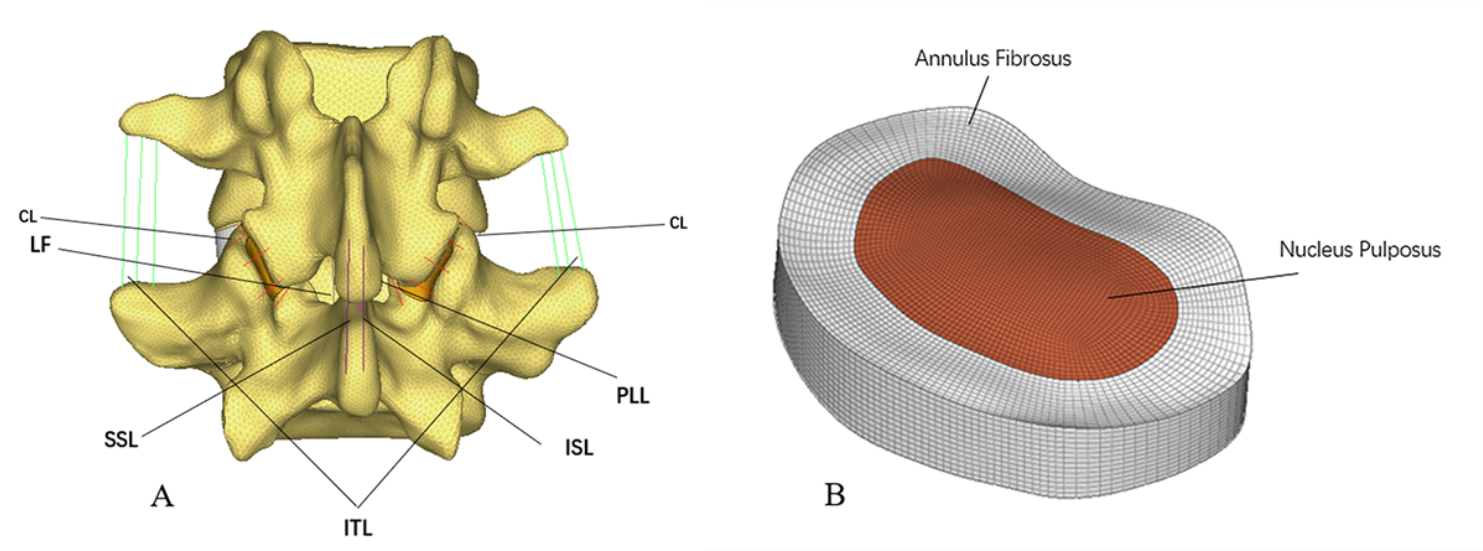

Figure 1

A The finite element model of the L4-L5 segment including the vertebrae, seven spinal ligaments, and intervertebral disc. **B** Annulus fibrosus and nucleus pulposus.

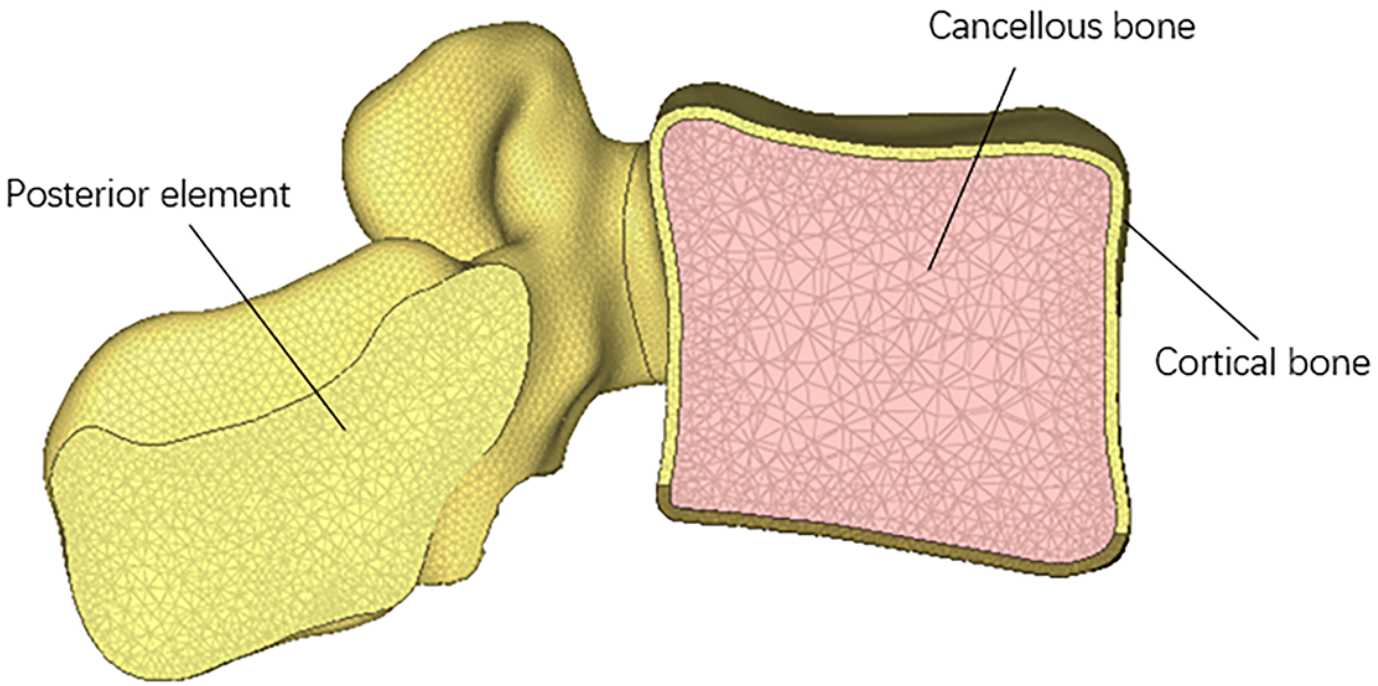

Figure 2

Cortical and cancellous bone

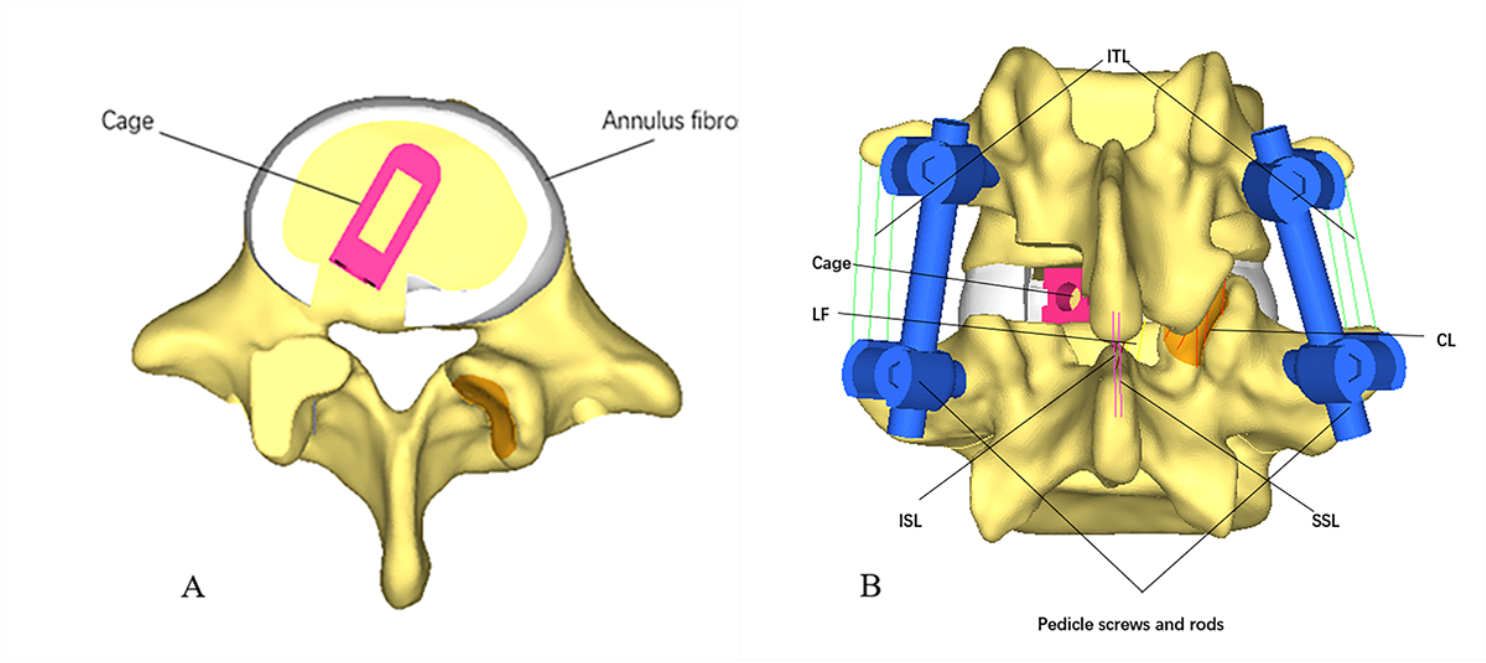

Figure 3

A Cage implantation in L4-5 intervertebral space. **B** Finite element model of UBE-LIF surgery

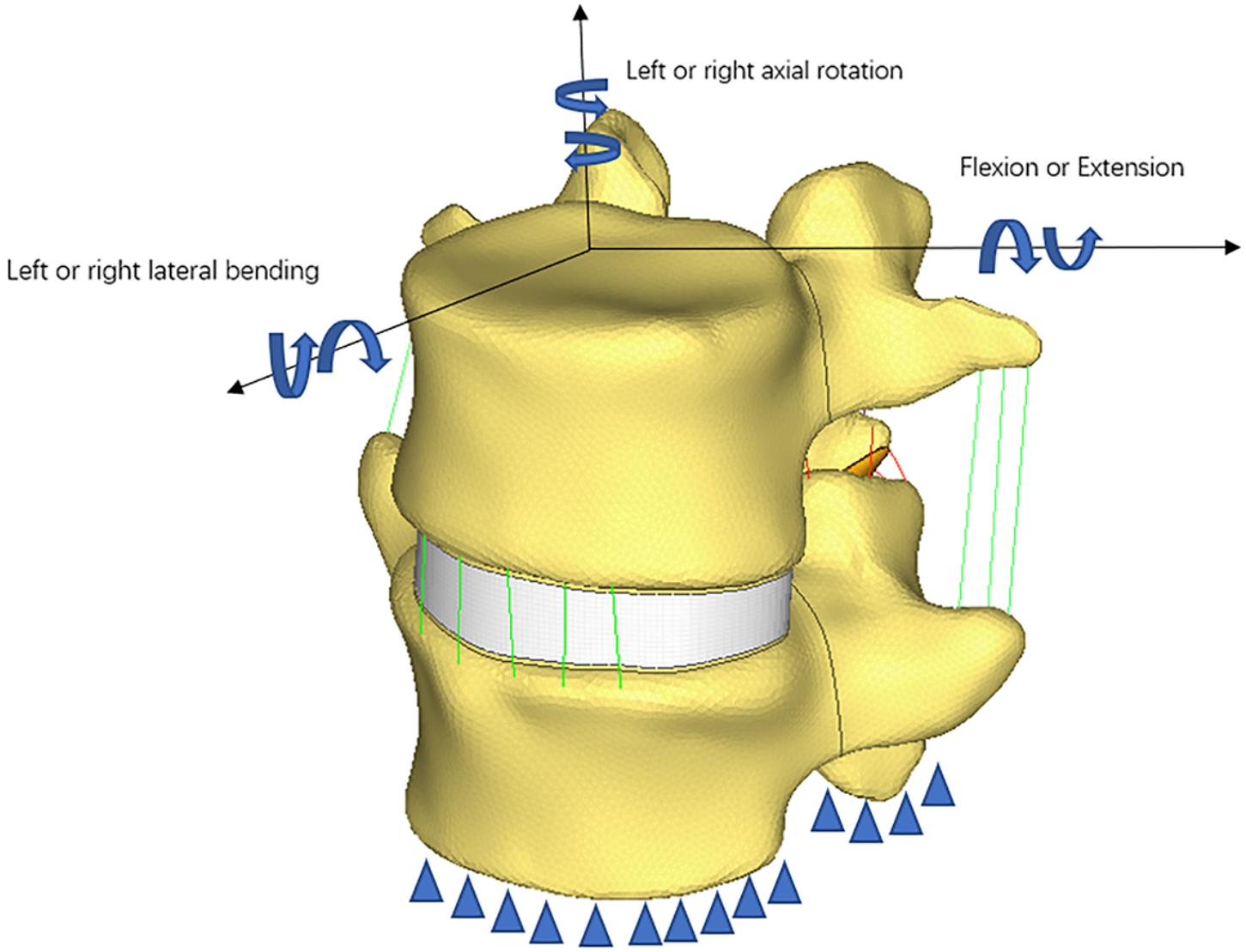

Figure 4

Application of the follower-load and physiological moments on the superior endplate of L4 while the inferior endplate of L5 was fixed

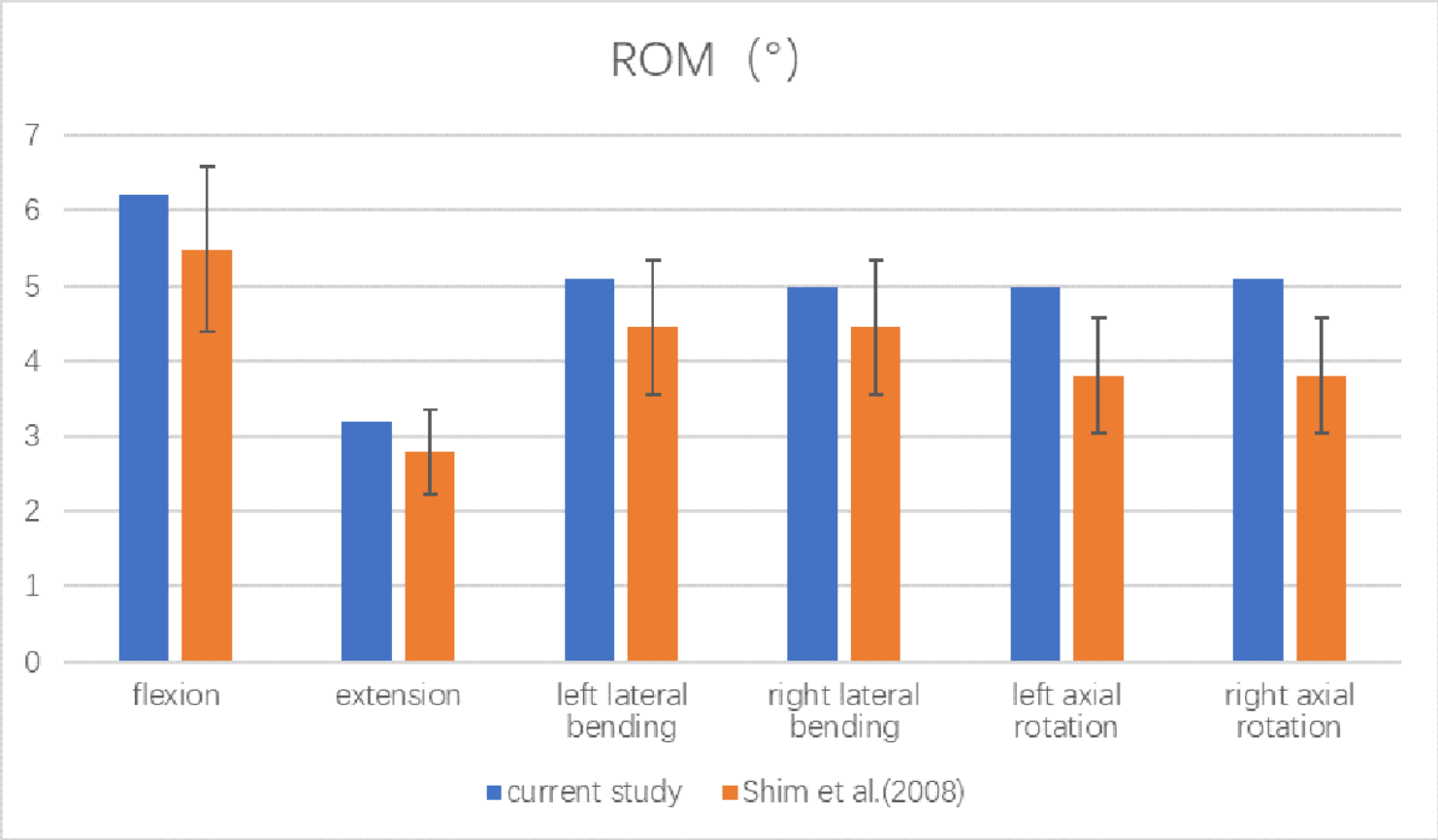

Figure 5

ROMs of the L4-5 finite element model at various positions

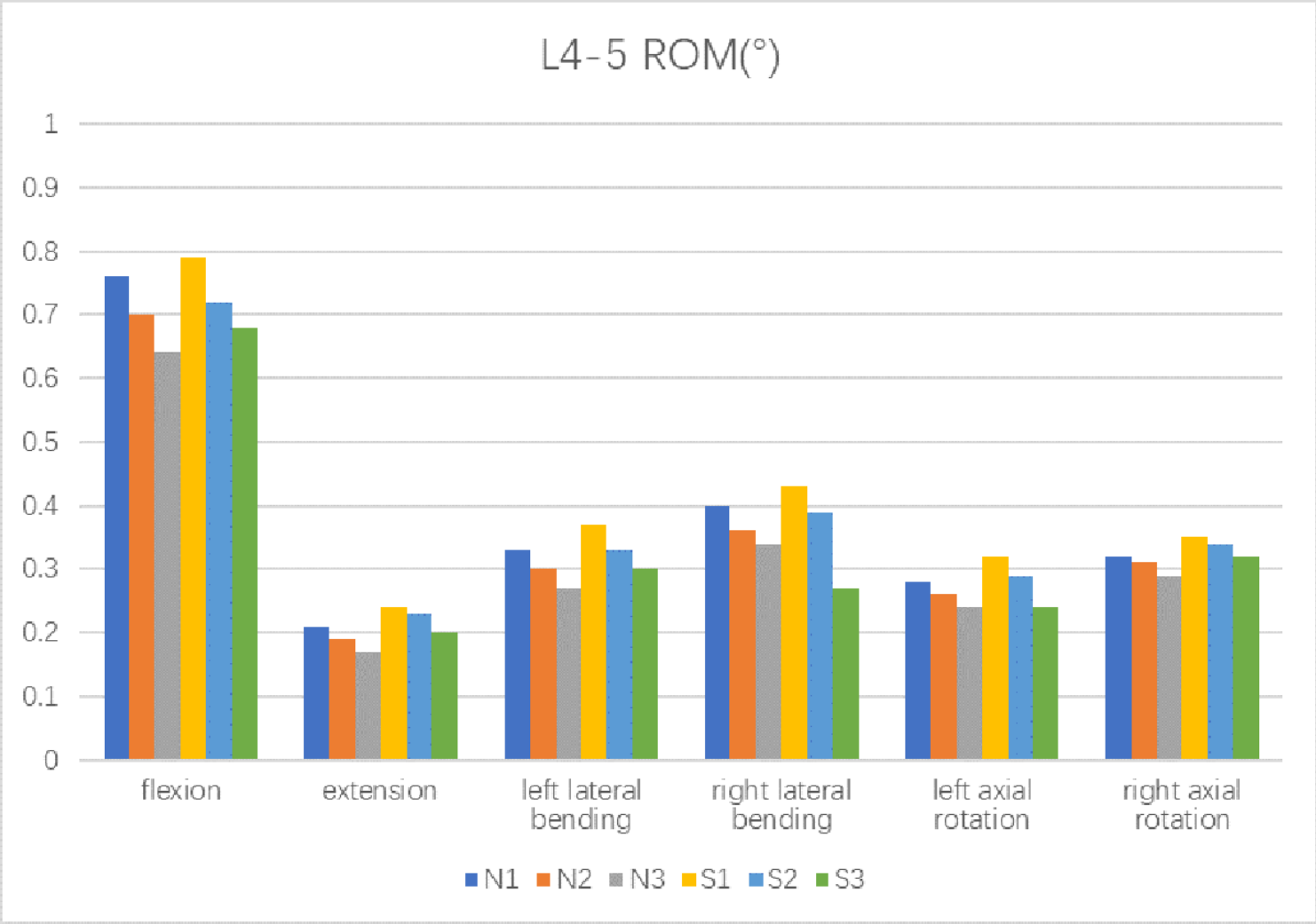

Figure 6

ROMs of the 6 surgical models at different body positions

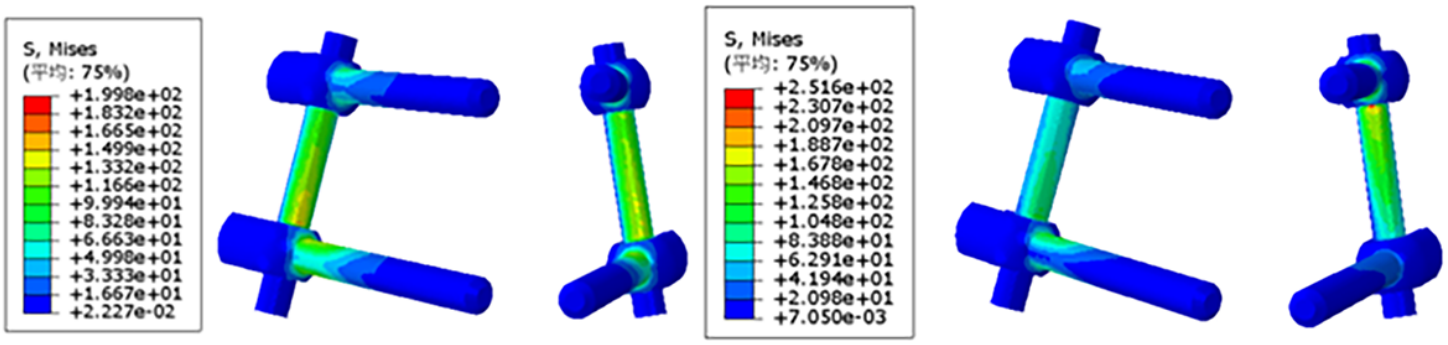

Figure 7

Stress (in MPa) on pedicle screw-rod system under simulated flexion moment of 10 N m and 500 N follower-load.

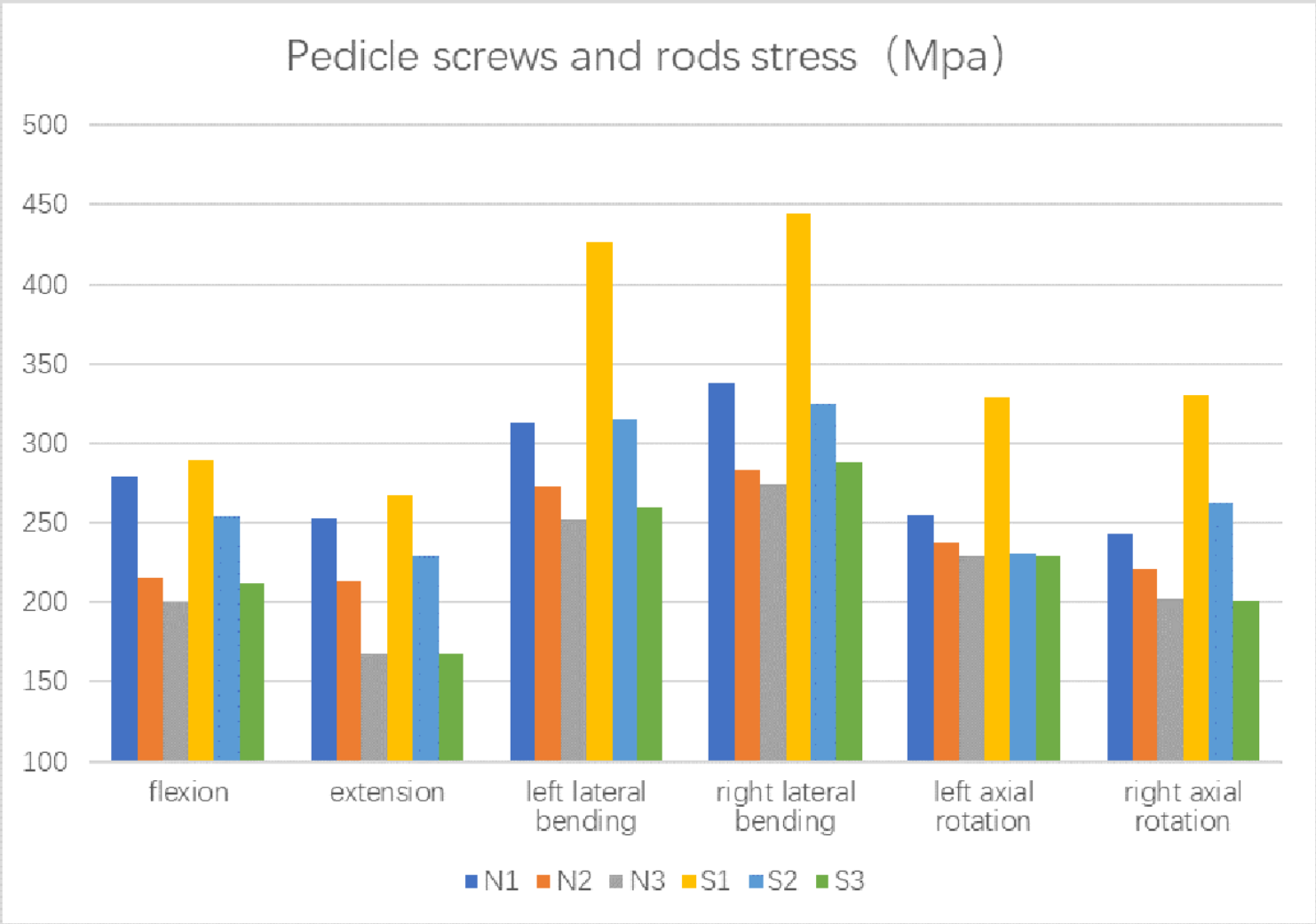

Figure 8

Stress of the Pedicle screw-rod system in each position of 6 surgical models

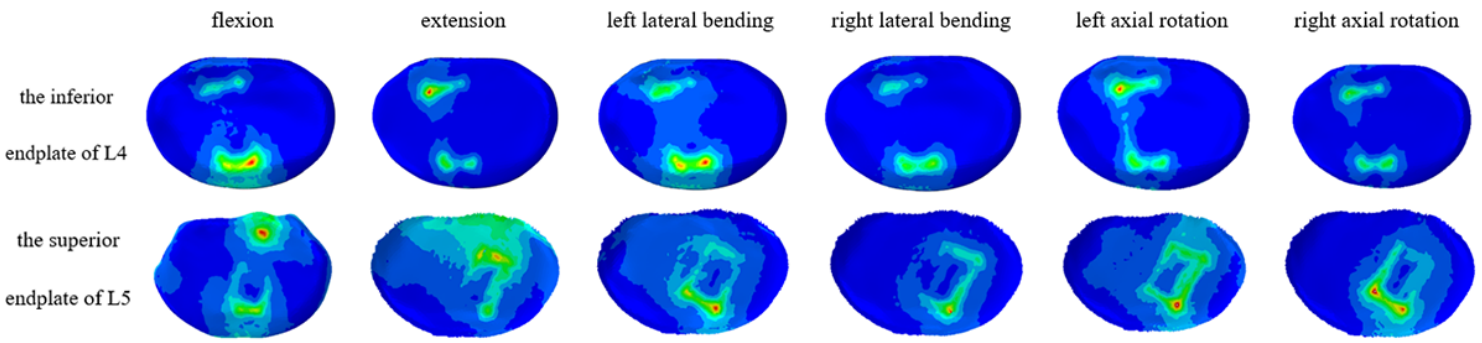

Figure 9

Stress (in MPa) on the inferior endplate of L4 and the superior endplate of L5 under simulated flexion moment of 10 N m and 500 N follower-load.

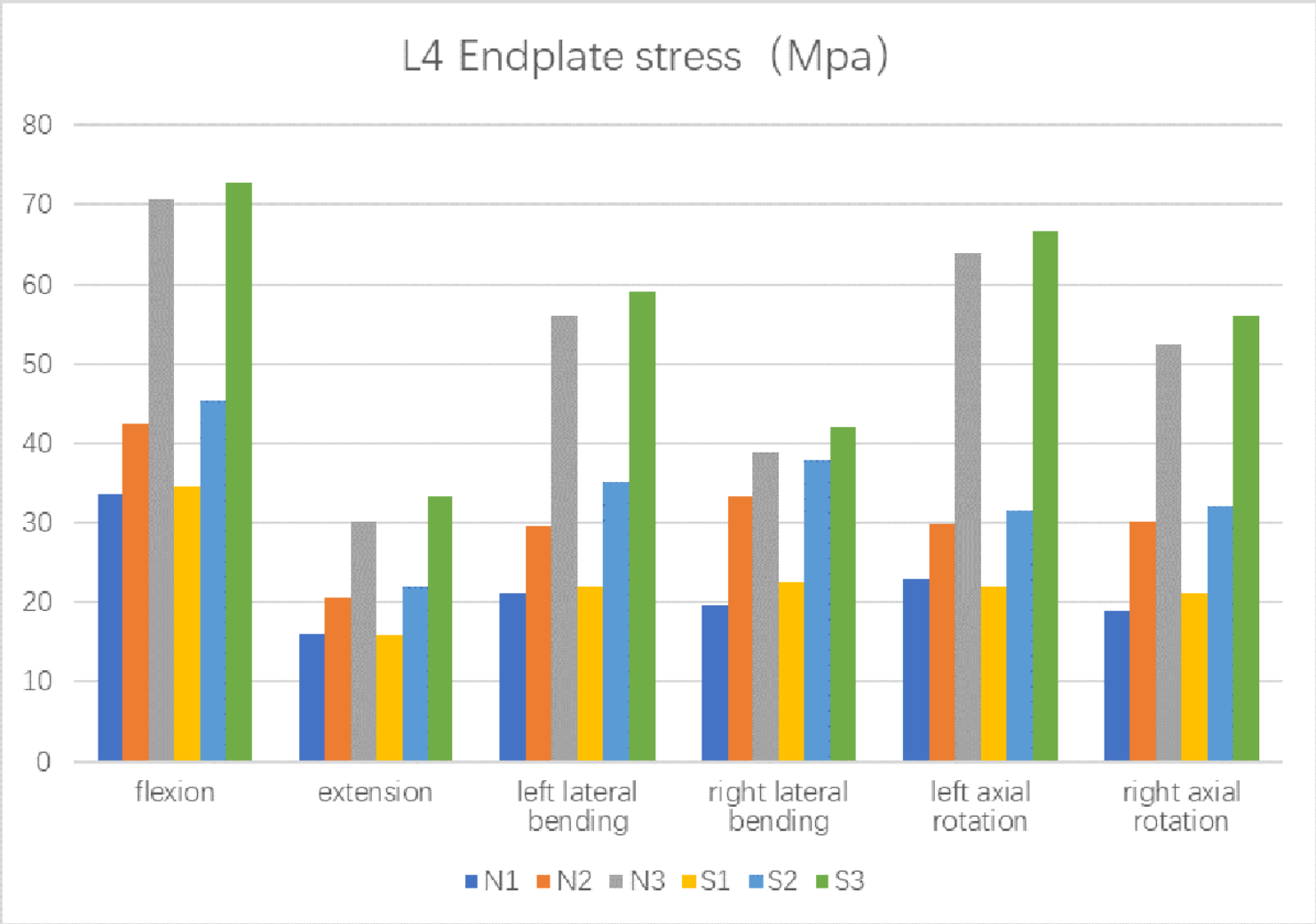

Figure 10

Stress of the L4 endplate at different positions in 6 surgical models

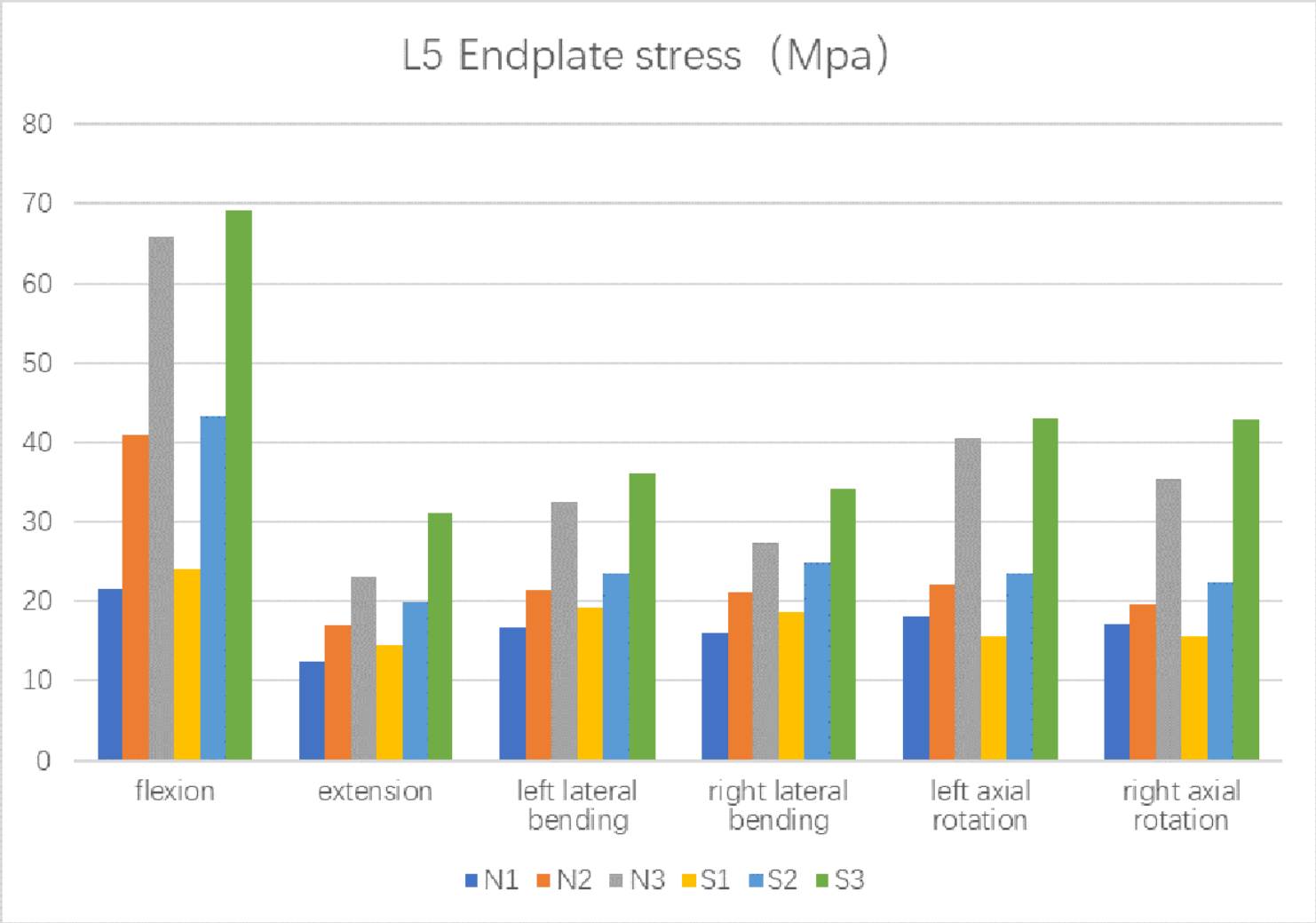

Figure 11

Stress of the L5 endplate at different positions in 6 surgical models